Draft version November 30, 2023
Typeset using LaTeX **manuscript** style in AASTeX63

Weak Solar Radio Bursts from the Solar Wind Acceleration Region Observed by Parker Solar Probe and Its Probable Emission Mechanism

Ling Chen,[1,2,3] Bing Ma,[1] Dejin Wu,[1,3] Xiaowei Zhou,[1] Marc Pulupa,[4] PeiJin Zhang,[5,6] Pietro Zucca,[6] Stuart D. Bale,[4,7,8,9] Justin C. Kasper,[10,11] and SuPing Duan[2]

[1] *Key Laboratory of Planetary Sciences, Purple Mountain Observatory, Chinese Academy of Sciences, Nanjing 210023, People's Republic of China*

[2] *State Key Laboratory of Space Weather, Chinese Academy of Sciences, Beijing 100190, People's Republic of China*

[3] *CAS Center for Excellence in Comparative Planetology, Hefei 230026, People's Republic of China*

[4] *Space Sciences Laboratory, University of California, Berkeley, CA 94720-7450, USA*

[5] *Department of Physics, University of Helsinki, PO Box 64, 00014 Helsinki, Finland*

[6] *ASTRON, The Netherlands Institute for Radio Astronomy, Oude Hoogeveensedijk 4, 7991 PD Dwingeloo, The Netherlands*

[7] *Physics Department, University of California, Berkeley, CA 94720-7300, USA*

[8] *The Blackett Laboratory, Imperial College London, London, SW7 2AZ, UK*

[9] *School of Physics and Astronomy, Queen Mary University of London, London E1 4NS, UK*

[10] *BWX Technologies, Inc., Washington, DC 20001, USA*

[11] *Climate and Space Sciences and Engineering, University of Michigan, Ann Arbor, Michigan 48109, USA*

(Received ??; Revised ??; Accepted ??)

Submitted to ApJL

ABSTRACT

The Parker Solar Probe (PSP) provides us the unprecedentedly close approach observation to the Sun, and hence the possibility of directly understanding the "elementary

Corresponding author: Ling Chen
clvslc214@pmo.ac.cn

process" which occurs in the kinetic scale of particles collective interactioin in solar coronal plasmas. We reported a kind of weak solar radio bursts (SRBs), which are detected by PSP when it passed a low-density magnetic channel during its second encounter phase. These weak SRBs have low starting frequecny ~ 20 MHz and narrow frequency range from a few tens MHz to a few hundres kHz. Their dynamic spectra display a strongly evolving feature of the intermediate relative drift rate decreasing rapidly from above 0.01/s to below 0.01/s. Analyses based on common empirical models of solar coronal plasmas indicate that these weak SRBs originate from the heliocentric distance $\sim 1.1 - 6.1\ R_S$ (the solar radius), a typical solar wind acceleration region with a low-β plasma, and indicate that their soruces have a typic motion velociy $\sim v_A$ (Alfvén velocity) obviously lower than that of fast electrons required by effectively exciting SRBs. We propose that solitary kinetic Alfvén waves with kinetic scales can be responsible for the generation of these small-scale weak SRBs, called solitary wave radiation (SWR).

Keywords: Solar radio emission, Interplanetary physics

1. INTRODUCTION

Solar radio bursts (SRBs) are the most direct manifestation of energetic electrons, which exist ubiquitously in the solar atmosphere although their origin remains poorly understood. It has been commonly believed that the ordinary type III and the type V SRBs are generated by energetic electrons via the process of magnetic reconnection during solar flare. The type II and the moving type IV SRBs are believed to be triggered by CME-associated shock accelerated electrons. The dynamic spectra of SRBs can provide the sensitive and rich information of solar energetic electrons as well as of the background plasma in the emitting source regions (Wild 1950; Wild et al. 1954; Lin et al. 1973; Melrose 1980; Chen et al. 2017). For instance, a fast frequency drift of dynamic spectra of type III SRBs, characterized by a relative frequency-drift rate $D \equiv \mid (df/dt)/f \mid > 0.1/s$ (f the emitting frequency), directly indicates the travelling velocity of fast electron beams (FEBs) of emitting type III SRBs. The dynamic spectra of type II SRBs usually present a slow drift with

$D < 0.01/s$ caused by the energetic electrons accelerated by the CME driven shock. Moreover, the dynamic spectra of moving type IV SRBs display often a very slow drift with $D \ll 0.01/s$ that can be attributed to the sub-Alfvénic motion of coronal loops, in which energetic electrons are trapped (Tan et al. 2019).

For type III SRBs, using observations made by the Geotail and Akebono satellites, micro-type III bursts characterized by short lifetime, continuous, and weak emission are found by Morioka et al. (2007, 2015). They showed that micro-type III bursts have a distribution of emitted power flux that is different from that of ordinary type III bursts, and concluded that they are not just weaker versions of the ordinary bursts. Owing to PSP's close distance to the Sun, PSP/IS$\odot$IS observed a rich array of energetic particle events, which were not observed by the spacecraft at 1 AU, over the first two orbits (McComas et al. 2019). Ma et al. (2022) also found that, because of the radiation attenuation effect, many weak type III-like bursts with a higher cutoff frequency (hence narrower bandwidth) clearly detected by PSP can hardly be observed by WIND when PSP approaches its perihelion. In the microwave frequency range, the radio bursts called solar microwave drifting spikes, which are characterized typically by a short lifetime (∼tens of ms), and an intermediate frequency drift rate (∼a few hundred of MHz/s), have been detected by the Solar Broadband Radio Spectrometer of the National Astronomical Observatories of China. Wu et al. (2007) suggested that these Solar microwave drifting spikes probably are produced by accelerated electrons trapped within solitary kinetic Alfvén waves (SKAWs) potential well and the intermediate frequency drifts are attributed to the SKAWs propagation along the magnetic field.

Here, we report a kind of weak SRBs, which were found in recent observations of the Parker Solar Probe (PSP) when it passed through a magnetic channel with low density at a heliocentric distance of $\sim 36\ R_S$ (the solar radius) during its second encounter around the Sun (Fox et al. 2016; Pulupa et al. 2017, 2020; Ma et al. 2021). These weak SRBs can be characterized by a weak intensity, low starting frequency, narrow frequency range, and short lifetime, and probably originated from some small-scale emitting sources. Their dynamic spectra display a strongly evolving feature of that the relative drift rate decreases rapidly from $D > 0.01/s$ to $D < 0.01/s$ when the emitting frequency drifts downward

from a few tens MHz to a few hundreds kHz. Based on common empirical models of solar coronal plasmas (Mariani & Neubauer 1990; Leblanc et al. 1998; Wu & Fang 2003; Wu & Yang 2007), the observation of PSP shows that the emitting sources travel along the low-density magnetic channel (or called equatorial coronal hole following ref. Bale et al. (2019)) towards from the heliocentric distance $R \sim 1.1\ R_S$ to $R \sim 6.1\ R_S$, a typical region of the solar wind acceleration.

The active region (AR) 12737, which is possibly associated with the low-density magnetic channel observed by PSP, does not have evident flare or jet activities during the corresponding time period. In addition, there is no obvious Hard-X ray emission based on the observation of Fermi. Hence, it seems that the energetic electrons responsible for these weak SRBs not come directly from flare or jet activities in the AR 12737. However, in a low-β plasma with $v_A > v_{T_e}$, where v_A is the Alfvén velocity and v_{T_e} is the electron thermal velocity, SKAWs can travel at a velocity higher than v_A and their electric fields may accelerate electrons to a velocity much higher than v_A and trap these energetic electrons within their potential wells. These trapped energetic electrons can generate coherent radio radiation via the electron cyclotron maser (ECM) instability. In particular, the propagation and evolution of SKAWs can reasonably explain the frequency drifting feature in the dynamic spectra of these weak SRBs. Therefore, we propose that the kinetic-scale SKAWs can be responsible for the generation of the weak small-scale SRBs observed by PSP, called solitary wave radiation (SWR). The rest of the paper is organized as follows. In Section 2, the main observed properties of weak SRBs detected by PSP during its crossing of the low-density magnetic channel and the correspongding solar wind plasma parameters are presented. Then, combining the in situ measurement of PSP and the empirical model of solar atmospheres, we foucus on discussing the generation mechanism of those weak SRBs in Section 3. Finally, summary and discussion are given in Section 4.

2. PSP OBSERVATION AND DATA ANALYSIS

NASA's PSP (Fox et al. 2016) was launched into a heliocentric orbit on 2018 August 12 and will fly closer to the Sun than any other spacecraft before it. The primary science goals for this mission are to trace the energy flow from the solar corona to the solar wind and to help us understand the solar corona heating and the solar wind acceleration. In particular, PSP is the first spacecraft to do in situ

measurements of the solar corona and the source region of the solar wind. To accomplish these science goals, four scientific instruments are carried by PSP: Fields Experiment (FIELDS; (Bale et al. 2016)), Solar Wind Electrons Alphas and Protons investigation (SWEAP; (Kasper et al. 2016)), Integrated Science Investigation of the Sun (IS⊙IS; (McComas et al. 2016)), and Wide-field Imager for Solar PRobe (WISPR; (Vourlidas et al. 2016)). Data presented in this study are mainly made by the FIELDS experiment designed to do measurements of electric and magnetic fields. The radio data are obtained by the Radio Frequency Spectrometer (RFS) (Pulupa et al. 2017) with the dual-channel receiver, the Low Frequency Receiver (LFR): 10.5 kHz-1.7 MHz and the High Frequency Receiver (HFR): 1.3 MHz-19.2 MHz.

The weak SRBs reported in this work were observed by PSP during its second solar encounter (E02) from April 3 to 6, 2019, as shown in Figure 1, in which panel (a) displays the power spectral density (PSD) of the radio radiation, covering the frequency band from 10.5 kHz to 19.2 MHz. Panels (b) and (c) in Figure 1 present the magnetic field (B) and its three components in the R-T-N frame (B_R, B_T, and B_N), and panels (d) and (e) do the solar wind velocity (v_p) and its components (v_{pR}, v_{pT}, and v_{pN}). Plasma density (n_e) and temperature (T_p) are exhibited in panels (f) and (g), respectively, and the final panel (h) shows the heliocentric distance of PSP in units of the solar radius R_S. From Figure 1, one can find that in the light yellow region between 08:08:34 UT on April 3 and 13:17:09 UT on April 6, 2019, the magnetic field B strengthens mainly in its radial component B_R from ~ 80 nT at the edge to > 100 nT in the center, and on the contrary the density n_e significantly reduces from > 400 cm^{-3} at the edge to ~ 100 cm^{-3} in the center, as shown in the panels (b-c) and in the panel (f), respectively. This implies that PSP was crossing a low-density magnetic channel at the heliocentric distance ~ 36 R_S. On the other hand, the panel (g) and the panels (d-e) show that the plasma temperature (T_p) and flow velocity (v_p, mainly its radial component v_{pR}), increase considerably from ~ 10 eV and ~ 250 km/s at the edge to ~ 30 eV and ~ 450 km/s in the center, respectively, implying that the plasma is heated and accelerated to form a solar wind stream in the center of this open magnetic channel.

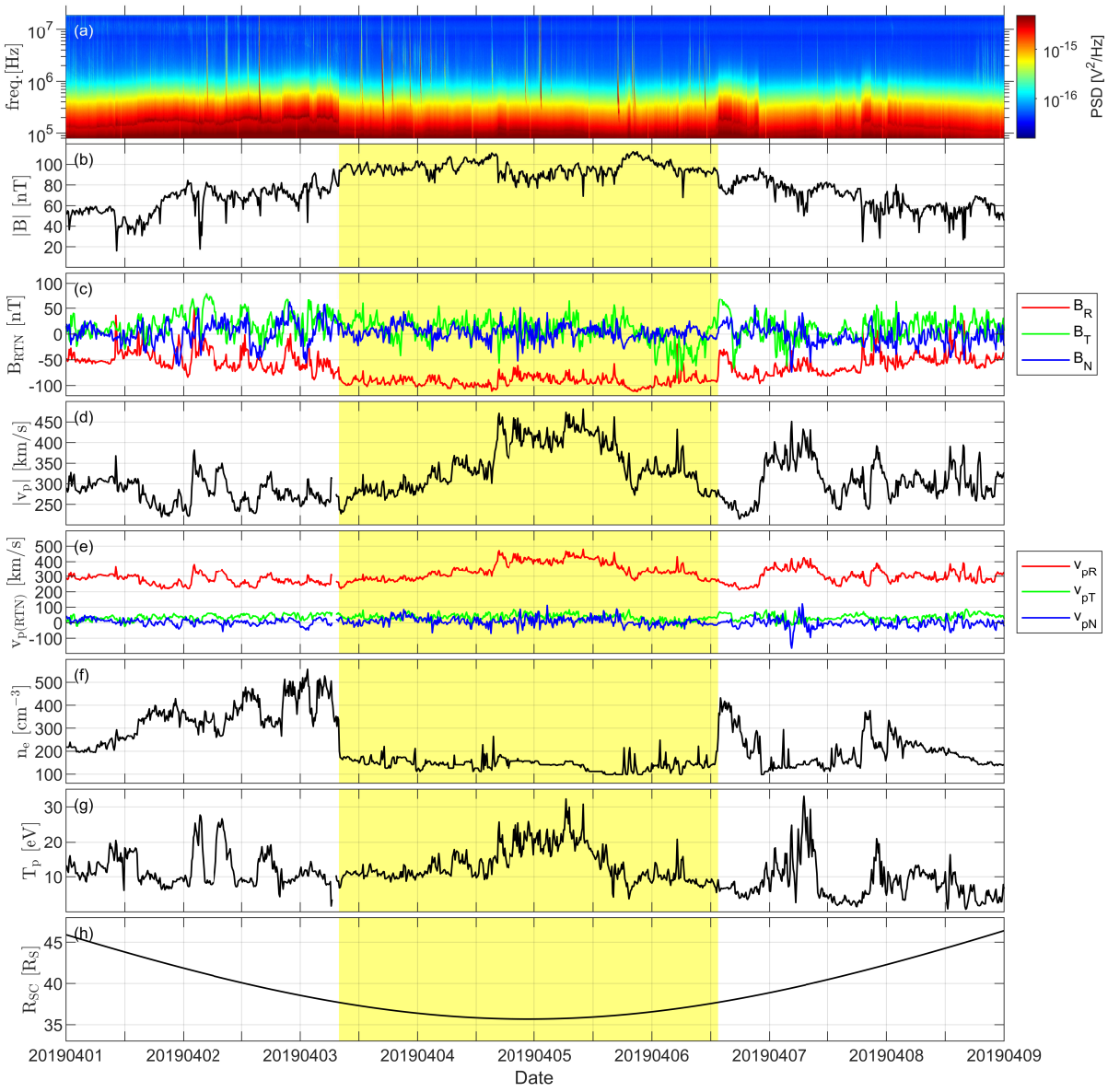

Figure 1. (color online) The solar wind plasma parameters observed by PSP between April 1 and 9, 2019. From top to bottom, panels are the power spectral density (PSD) of the radio radiation (a), the magnetic field (b) and its components (c), the solar wind velocity (d) and its components (e), the plasma density (f) and temperature (g), and the heliocentric distance of PSP in units of the solar radius R_S (h), respectively. A low-density magnetic channel is clearly displayed between 08:08:34 UT on April 3 and 13:17:09 UT on April 6, 2019 (see the light yellow region).

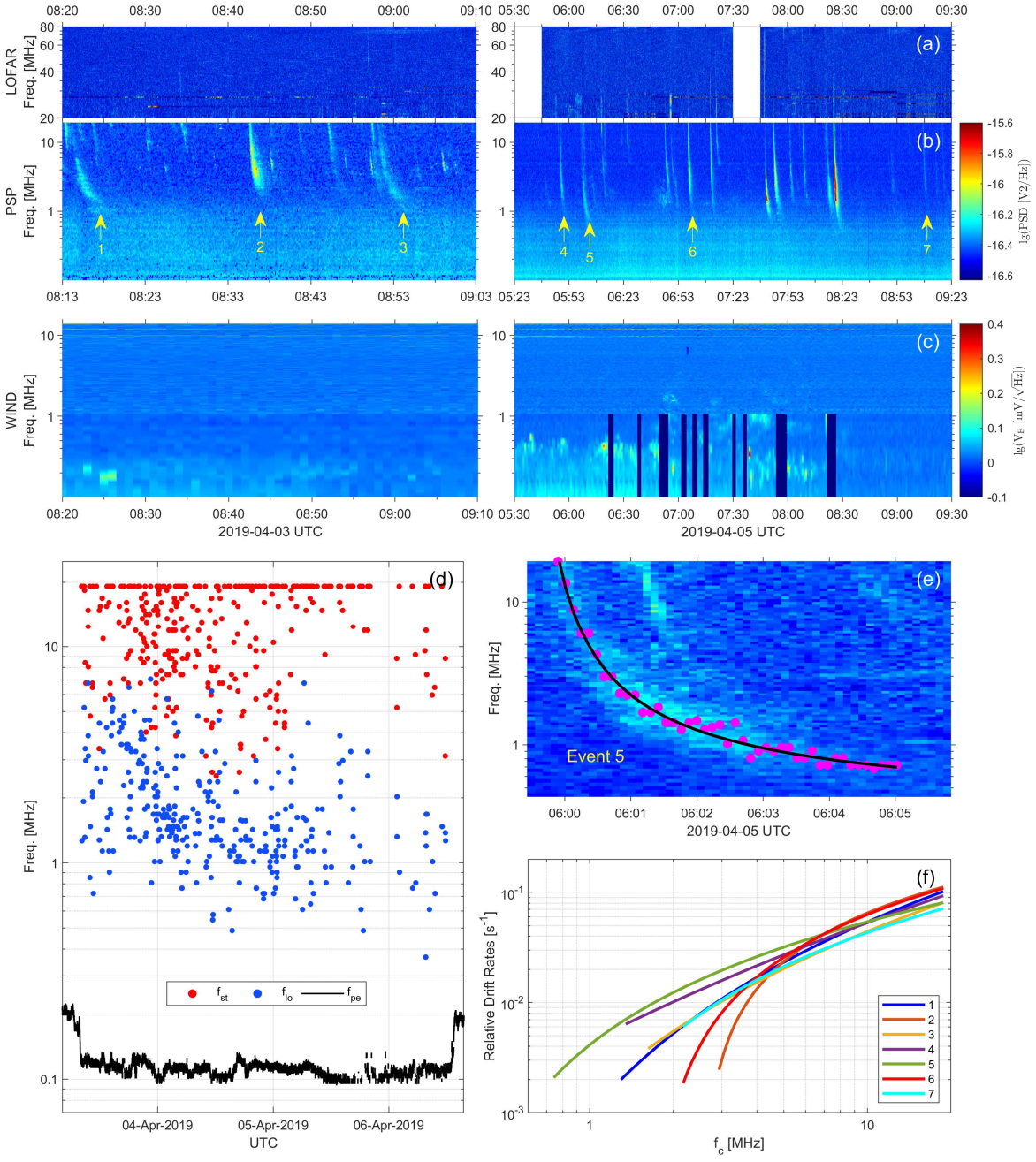

Figure 2. (color online) The weak SRBs observed by PSP during its crossing of the low-density magnetic channel. The top three rows show PSD measured by LOFAR (a), PSP (b), and WIND (c) in two intervals 08:13 to 09:03 on April 3, 2019 (left) and 05:23 to 09:23 on April 5, 2019 (right). (d) The starting (f_{st}, red circles) and ending (f_{lo}, blue circles) frequencies for the 385 weak SRBs, and the local plasma frequency f_{pe} (back line) along the PSP orbit. (e) The fitting curve (black curve) of maximal PSD for event 5 marked by arrow in the panel (b) through the least square fit, where the magenta dots are the location of maximal PSD in the dynamic spectrum. (f) The relative frequency-drift rate for the several typical bursts as marked by arrows in the panel (b).

As seen in Figure 1(a), a large number of SRBs presented in the observation of PSP during its crossing of the low-density magnetic channel. We identified 428 SRBs with peak intensities between $10^{-12.6} - 10^{-16.3}$ V^2/Hz, above well the sensitivity of the RSF measurement, $\sim 10^{-18}$ V^2/Hz (Pulupa et al. 2017). Among these identifiable SRBs only 43 bursts ($\sim$ 10%) have peak intensities higher than 10^{-15} V^2/Hz, and all the rest 385 bursts have peak intensities lower than 10^{-15} V^2/Hz. These very weak SRBs have a rather high occurrence rate of $\sim$ five bursts per hour in average and they can be regarded as point sources and should originate from small-scale emitting sources because of their weakness. In the panel (d) of Figure 2, the starting (f_{st}) and ending (f_{lo}) frequencies of these weak SRBs are displayed by red and blue circle dots, respectively. The local plasma frequency f_{pe} along the PSP orbit is presented by the black line. One can see that the lowest ending frequency ($f_{lo} = 367$ kHz) of these weak SRBs is well higher than the local plasma frequency $f_{pe} \sim 100$ kHz, implying that they all had stopped radiating before arriving at PSP. The starting frequencies of 247 weak SRBs ($\sim$ 64%) can be determined definitely because their f_{st} all are well lower than the upper-limit frequency of the RFS measurement (i.e., $\sim$ 19.2 MHz). Other about one third (138 events) weak SRBs, however, have f_{st} reaching the upper-limit frequency of the RFS measurement as shown in Figure 2(d), which indicates that their actual starting frequencies possibly are higher than 19.2 MHz.

In order to find their real starting frequencies, we further compared the PSP observation with that by LOFAR (the Low-Frequency Array in Europe) during the same interval, which has an effective-observation frequency range between 20–80 MHz. However, due to limited observation time of LOFAR allocated for solar and spaceweather division, only 151 of these 385 weak SRBs occurred in the solar observation windows of LOFAR. The result showed that only less than one fourth (36 of the 151 SRBs) have $f_{st} > 20$ MHz and hence were observed by LOFAR. Figure 2 shows further the comparison between observations of LOFAR (a), PSP (b), and WIND (c) for two intervals 08:13 to 09:03 on April 3, 2019 (left) and 05:23 to 09:23 on April 5, 2019 (right), in which there are 5 (left) and 16 (right) weak SRBs, respectively. In the panels (a) and (c) of Figure 2 an 7-minutes delay for LOFAR and WIND is due to the consideration of the radiation propagation from PSP to LOFAR

and WIND. In the comparison with the LOFAR observation, only part bursts extend their emission to frequencies higher than 20 MHz as seen in Figure 2(a). In the WIND observation, however, almost all these weak SRBs are invisible because of their weakness as seen in Figure 2(c). In fact, only some strong SRBs with the peak intensity higher than 10^{-15} V^2/Hz can be seen by WIND, and these strong SRBs, in general, also have a higher starting frequency in the LOFAR observation.

The relative frequency-drift rate is an important and critical parameter that reflects directly the environment and motion of the emitting source in the background plasma. It has been used as a typically characteristic parameter to classify various kinds of SRBs. Here, we take the event 5 marked by arrow in Figure 2(b) as an example to show the determination of the relative frequency-drift rate D. After subtracting the background noise, the dynamic spectrum of the event 5 is shown in Figure 2(e), in which at the low frequencies (∼1 MHz or below) the burst becomes more clear compared to the background. By finding the frequencies of maximal PSD (magenta dots) of the event 5 at each time point, we can obtain the fitting curve (black curve) for the frequency-time relation in a polynomial form, $\lg f = at^b + c$, with the parameters $a = 5.722$, $b = -0.704$, and $c = 5.474$ for the event 5, which are obtained by the least square fit. Then, the relative frequency-drift rate can be calculated by the expression of the fitting curve. The advantage of this method is to avoid limiting by lower time resolution around the highest frequencies (∼19 MHz) in the determination of drift rate. Figure 2(f) shows the relative frequency-drift rate D versus the central frequency for the several typical examples marked by arrows in Figure 2(b), and the result shows that their relative drifting rates have an initial value lower than and close to $\sim 0.1/s$ and rapidly slow down from $> 0.01/s$ to $< 0.01/s$ as the emitting frequency drifts downward from a few tens MHz to a few hundreds kHz. This implies that their emitting sources probably experienced strong dynamical evolutions. An interesting and puzzling question is where the energetic electrons responsible for these weak SRBs come from, which should exist rather ubiquitously.

On the other hand, combining the remote sensing observations by the Hinode EUV Imaging Spectrometer and the Solar Dynamics Observatory Atmospheric Imaging Assembly, Harra et al. (2021) found that the active region (AR) 12737 is possibly associated with the low-density magnetic chan-

nel observed by PSP. The AR 12737, however, does not have evident flare or jet activities during the corresponding time period. Based on the observation of Fermi, there is also no obvious Hard-X ray emission. Therefore, it seems to be unlikely that FEBs responsible for these weak SRBs come directly from flare or jet activities in the AR 12737. In addition, there is an extended blue-shifted outflow region inside the AR 12737, and its expanding behavior probably leads to the formation of the low-density magnetic channel and the solar wind stream. Moreover, the solar wind magnetic field is dominated by the radial component B_R and follows a similar Parker spiral structure (Parker 1958). Therefore, it is a reasonable inference that the magnetic channel extends from the AR 12737 in the solar corona to the solar wind. Accompanied with the acceleration and heating of the solar wind, the emitting sources of these weak SRBs were formed and travelled outwards along this magnetic channel (Reiner & Kaiser 1999; Ma et al. 2021). In particular, the rapid decrease of their relative drifting rates indicates that their emitting sources should have experienced strong dynamic evolutions in the solar wind acceleration region.

3. PLASMA PARAMETERS MODEL AND GENERATION MECHANISM OF WEAK SRBS

3.1. *Plasma Parameters Model*

Both the emitting source and the emission mechanism of these weak SRBs sensitively depend on the local plasma parameters in the source region. For example, their emitting frequencies are associated closely to be the characteristic frequencies of the local plasma in the source regions, such as the plasma frequency $f_{pe} = 8.98\sqrt{n_e}$ kHz for the plasma emission and the electron cyclotron frequency $f_{ce} = 2.8B_0$ MHz for the ECM emission, where the ambient plasma density n_e and magnetic field B_0 are in units of cm^{-3} and Gauss, respectively. The relative frequency-drift rate D of the dynamic spectra, in general, can be determined by the moving velocity of the emitting source and the variation of the characteristic frequencies (f_{pe} or f_{ce}), which are given directly by the ambient plasma density (n_e) or magnetic field (B_0) along the propagation path of the weak SRBs.

A widely adopted model for the radial distribution of the average plasma density from the solar corona at $\sim 1.8\ R_S$ to the solar wind at ~ 1 AU is the polynomial distribution proposed by

Leblanc et al. (1998), $n_e = a\,(242.5r^{-6} + 12.5r^{-4} + r^{-2})\,10^5$ cm^{-3}, in which r is the heliocentric distance in units of the solar radius R_S, the first and third terms proportional to r^{-6} and r^{-2} are dominant in the solar corona and the solar wind, respectively, the second term proportional to r^{-4} is used to fit the transition between the corona and the wind, and the coefficient a can be determined by the measured density value at 1 AU or other distances. In the low corona, however, the density gradient is very steep in the exponential fall way. In order to fit the density of $\sim 10^{10}$ cm^{-3} at the base of the corona, Wu & Fang (2003) introduced an exponential function with a scale height $h \sim 0.02\ R_S$, $10^{10}e^{-50(r-1)}$ cm^{-3}, to model the density distribution in the low corona. In addition, a density dilution factor, $d_f(r) \equiv \left[1 + 9e^{-(r-1)^2/100}\right]^{-1}$, may be invoked to describe the low-density feature of the magnetic channel (Esser & Sasselov 1999; Esser et al. 1999; Young et al. 1999; Teriaca et al. 2003; Wu & Yang 2007). In consequence, the radial distribution of the electron density along the magnetic channel can be fitted by

$$n_e(r) = d_f(r)\left[10^{10}e^{-50(r-1)} + (388r^{-4} + 20r^{-2} + 1.6)10^5 r^{-2}\right]\ (\mathrm{cm}^{-3}). \tag{1}$$

On the other hand, some numerical two-fluid models of high speed streams from the corona to the solar wind (Hu et al. 1997) showed that the radial distribution of the electron temperature can be characterized by a quick increase from $\sim 5 \times 10^5$ K to $\sim 1.5 \times 10^6$ K within $r < 3$, then a slow decrease by a factor of ~ 10 at a radial distance of about a few tens of R_S, followed by a slower decrease in the interplanetary space. Such temperature behavior may be described characteristically by

$$T_e(r) = \left[4.2re^{1-r/3} + 6(3r^{-1})^{0.3}\right]10^5\ (\mathrm{K}). \tag{2}$$

The radial distribution of the magnetic field along the magnetic channel can be modelled by the combination of a dipole field $\propto r^{-3}$ in the corona and a monopole field $\propto r^{-2}$ in the solar wind as (Mariani & Neubauer 1990),

$$B_0(r) = 15r^{-3} + r^{-2}\ (\mathrm{G}). \tag{3}$$

Here, the averaged electron density ($n_e \sim 120$ cm^{-3}), temperature ($T_e \sim 25$ eV), and magnetic field ($B_0 \sim 100$ nT) in situ measured by PSP at $\sim 36.6\ R_S$ (Halekas et al. 2020) have been used to fit the coefficients in the equations (1)–(3).

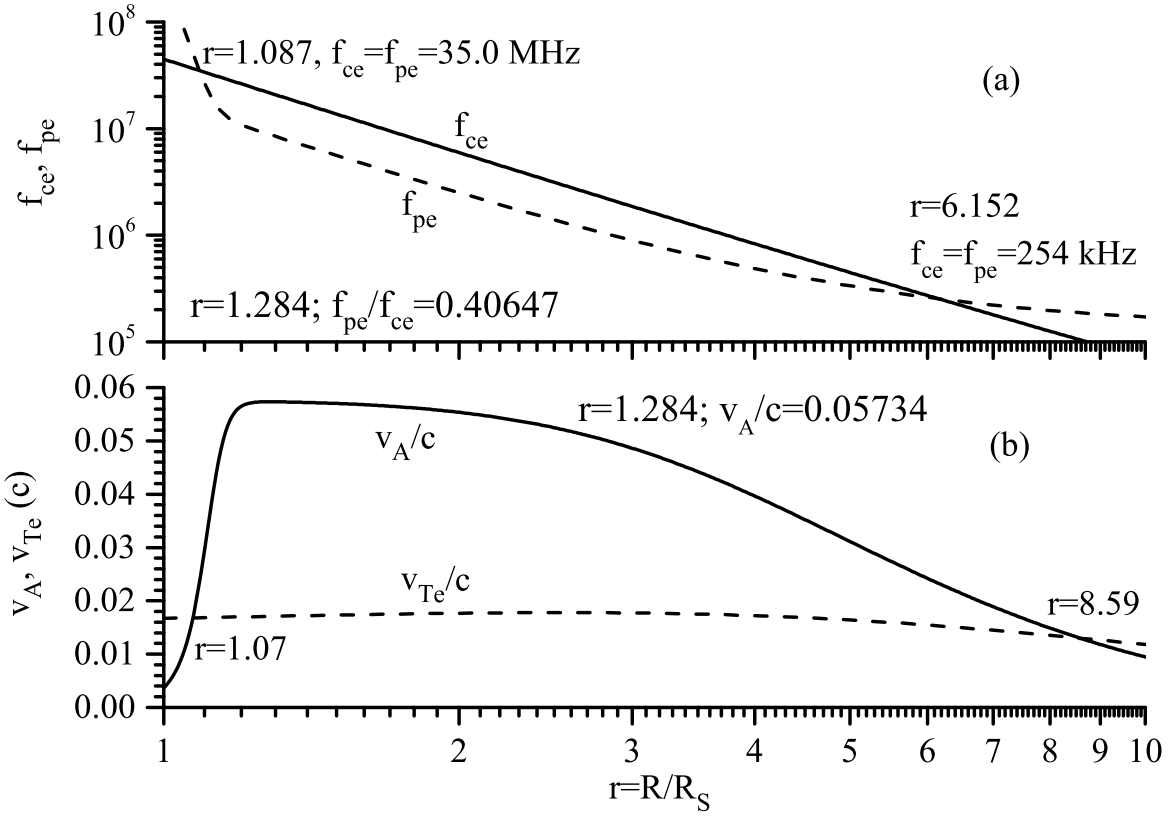

Figure 3. The radial distributions of characteristic frequencies and velocites. (a) The radial distributions of the electron cyclotron (f_{ce}) and plasma (f_{pe}) frequencies. (b) The radial distributions of the Alfvén (v_A) and electron thermal (v_{T_e}) velocities.

Based on the empirical models mentioned above, Figure 3(a) shows the radial distributions of the electron cyclotron ($f_{ce} = 2.8 \times 10^6 B_0(r)$ Hz; the solid line) and plasma ($f_{pe} = 8.98 \times 10^3 \sqrt{n_e(r)}$ Hz; the dashed line) frequencies, respectively. From Figure 3(a), it can be found that the low-density magnetic channel extends from $\sim$ 1.1 to $\sim$ 6.1 R_S in which the electron cyclotron frequency is evidently higher than the plasma frequency, that is, $f_{ce} > f_{pe}$ and the corresponding range of the

characteristic frequencies between $\sim$ 30 MHz and $\sim$ 300 kHz covers well the emitting frequency band of the weak SRBs. This further confirms that their emitting sources can be well located within the extended solar corona from $\sim$ 1.1 to $\sim$ 6.1 R_S, which is a low-density magnetic channel or an equatorial coronal hole with outflows and open magnetic fields. Usually, this extended coronal region is extensively believed to be the important region of the solar wind origin and acceleration.

Figure 3(b) presents the local Alfvén velocity v_A (solid line) and the electron thermal velocity v_{T_e} (dashed line) normalized by the light velocity c. From Figure 3(b) one has $v_A > v_{T_e}$ in the emitting source region of these weak SRBs ($\sim 1.1 - 6.1\ R_S$), implying there is a low-β plasma of $\beta < m_e/m_p$ in the source region, where m_e and m_p are electron and proton masses, respectively. Based on the theory of kinetic Alfvén waves (KAWs) (Wu 2012; Wu & Chen 2020), a low-β SKAW, accompanied by a dip density soliton with an inner density $n_{em} < n_0$, can propagate at a super-Alfvén velocity $v_{sw} = \sqrt{(2+n_m)/3n_m}v_A > v_A$ along the magnetic field, where $n_m \equiv n_{em}/n_0$ is the inner density normalized by the ambient density n_0. In particular, the field-aligned electric field $E_\parallel$ of SKAW can efficiently trap and accelerate electrons to a typical velocity $v_{ez} = (n_m^{-1} - 1)\, v_{sw}$, much higher than v_A for $n_m \ll 1$ (Wu 2012; Wu & Chen 2020). For example, for $n_m = 0.2$, one has $v_{sw} = \sqrt{11/3}v_A \simeq 1.915 v_A$ and $v_{ez} = 4v_{sw} \simeq 7.66 v_A$. This can provide an efficient acceleration mechanism for the local generation of energetic electrons that is required to excit the emissions of the weak SRBs.

3.2. *Emission mechanism of weak SRBs*

It is worth noting that the low-density magnetic channel has similar plasma conditions to the source region of the terrestrial auroral kilometric radiation (AKR, see e.g. refs. Mozer et al. (1980); Bryant (1990); Wu & Chao (2004)), in which the electron cyclotron frequency f_{ce} is higher than the plasma frequency f_{pe} and the Alfvén velocity v_A is larger than the electron thermal velocity v_{T_e}. The condition $f_{ce} > f_{pe}$ indicates that the coherent radio radiation at the cyclotron frequency and its harmonics can be effectively excited by the ECM instability.

The solar wind acceleration region, located in the extended solar corona at $\sim 1.1 - 10\ R_S$, is a complex dynamical transition region, where the coronal plasma is heated and accelerated into the solar

wind. Alfvén wave (AW) turbulence, originating from the photospheric turbulence and convection, plays an important role in the coronal heating and solar wind acceleration (Cranmer & Ballegooijen 2005; Cranmer et al. 2007). The AW turbulence, via the anisotropic turbulent cascade, period doubling and wave breaking (Goldreich & Sridhar 1995; Tsurutani et al. 2018), can extend into the kinetic scales of particles and become the kinetic AWs (i.e., KAWs). Meanwhile, in a low-β plasma of $v_A > v_{T_e}$, nonlinear solitary wavelets of KAWs (i.e., SKAWs), may be formed effectively because KAWs can be free from the heavy Landau damping when their phase speed ($> v_A$) is considerably larger than the electron thermal speed (v_{T_e}). SKAWs and their associated structures have been observed and identified extensively in near-earth space plasmas, such as in the auroral plasma. A number of studies both in observation and theory have shown that the nonlinear KAWs can play an important role in the field-aligned acceleration of electrons and the crossing-field heating of ions in the aurora plasma (Louarn et al. 1994; Wahlund et al. 1994; Wu et al. 1995; Chaston et al. 1999; Stasiewicz et al. 2000; Wu & Chao 2004). For the case of the solar corona, also it is found that SKAWs can be responsible for the anomalous anisotropic energization of minor heavy ions discovered by the Solar and Heliospheric Observatory (SOHO) in the extended solar corona of $\sim 1.5 - 5\ R_S$ (Wu & Yang 2007; Wu 2012; Wu & Chen 2020).

On the other hand, the field-aligned electric field of SKAWs has a typical dipole structure, which can accelerate electrons along the magnetic field and trap these energetic electrons inside the potential well. Some recent works have shown that the presence of AW turbulence may significantly influence the ECM instability (Wu et al. 2012; Wu 2014; Zhao et al. 2015; Chen et al. 2017, 2021). Recently Kasper et al. (2021) found that the strong AW turbulence exists not only in super-Alfvénic streams such as in the solar wind but also can present in the low-β solar corona with a sub-Alfvénic stream. They reported the spectrum of Alfvén turbulence measured by PSP during its eighth solar encounter (E08), which has a typical power spectral density from $\sim 10^6$ to 10^3 km^2/s^2/Hz and a spectral index $\sim -3/2$ for the inertial turbulence range from 0.002 to 0.2 Hz. An ambient Alfvén velocity $v_A \sim 450$ km/s indicates the relative energy density of the Alfvén turbulence $\delta_B \sim 2 \times 10^{-2}$ (Kasper et al. 2021). However, this relative strength expresses only an average turbulence level of AWs, while the

actual relative strength can vary dependently on cases in a wide range, say, 0.01 to 0.1, in the solar corona (Cranmer & Ballegooijen 2005).

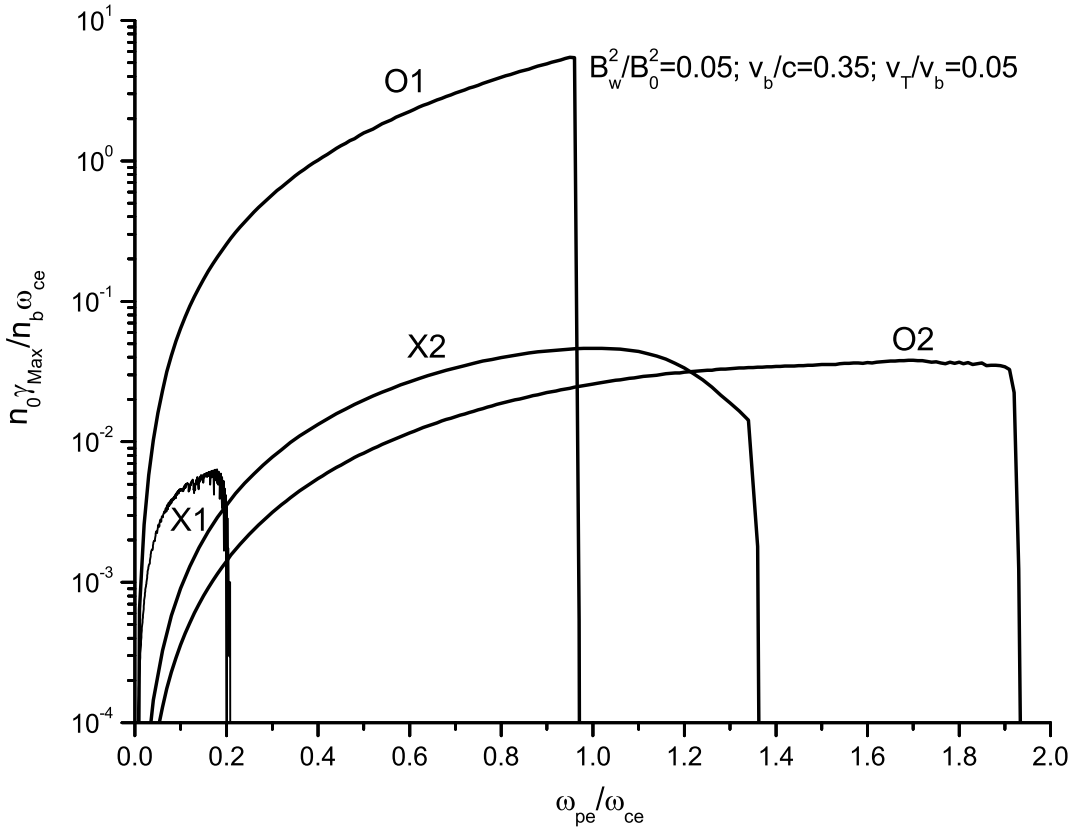

Figure 4. The growth rates of the ECM instability excited by the crescent-shaped distributions in Equation (4). O1 (X1) and O2 (X2) denote the ordinary (extraordinary) mode in the fundamental and harmonic frequencies, respectively. Parameters $\delta_B = 0.05$, $v_b/c = 0.35$, and $v_T/v_b = 0.05$ have been used.

Following Wu et al. (2012), the velocity distribution function of beam electrons with a characteristic beam velocity v_b under the influence of AW turbulence with the relative strength δ_B can be modelled by the so-called crescent-shaped distribution

$$f_b(v,\mu) = A \exp\left[-\frac{(v-v_b)^2}{v_T^2} - \frac{1-\mu^2}{\theta_\perp^2}\right], \tag{4}$$

where A is the normalization constant, $\mu \equiv v_z/v$ is the pitch angle of the electron velocity, v_T is the velocity spread of the beam electrons, and $\theta_\perp \equiv \sqrt{v_T^2/v_b^2 + 2\delta_B}$ is the pitch-angle spread of the beam electrons. In particular, the crescent-shaped distribution can effectively excite the ECM emission (Wu et al. 2012; Wu 2014; Zhao et al. 2015). Figure 4 shows the growth rates of the ECM instability versus the frequency ratio ω_{pe}/ω_{ce}, where the parameters $v_b = 0.35c$, $v_T = 0.05v_b$, and $\delta_B = 0.05$ have been used. As shown in Figure 4, the excited modes depend considerably on the frequency ratio ω_{pe}/ω_{ce}, in which the most easily excited emission is the fundamental ordinary mode (O1) in the low-β plasma of $\omega_{pe}/\omega_{ce} < 1$, while for the case of $1 < \omega_{pe}/\omega_{ce} < 2$, the harmonic waves of the ordinary (O2) and extraordinary (X2) modes also may be excited but at a much lower growth rate. However, the fundamental extraordinary mode (X1) can be excited only in the extreme condition of $\omega_{pe}/\omega_{ce} \ll 1$ because of its higher cutoff frequency than that of the ordinary mode.

As shown in Figure 3(a), in the low-density magnetic channel between ~ 1.1 and ~ 6.1 R_S, the exciting condition for the ECM emission, $\omega_{pe}/\omega_{ce} < 1$, can be satisfied and the frequency range between ~ 35 MHz and ~ 0.25 MHz covers well the emitting frequencies of the weak SRBs. Meanwhile, the low-β condition of $v_A > v_{T_e}$ in the emitting source region indicates that SKAWs with a dip density soliton can propagate at a super-Alfvén velocity $v_{sw} > v_A$ along the magnetic field (Wu 2012; Wu & Chen 2020). In particular, their field-aligned electric field $E_\parallel$ can efficiently accelerate electrons to form an oscillating energetic electron beam with a higher velocity $v_{ez} > v_{sw}$. For SKAW with a normalized inner density $n_m < 1$, the energetic electron beam can have a characterized beam velocity $v_b = v_{ez}$ (Wu 2012; Wu & Chen 2020), that is,

$$v_b = v_{ez} = \frac{1 - n_m}{n_m} v_{sw} = \frac{1 - n_m}{n_m} \sqrt{\frac{2 + n_m}{3n_m}} v_A. \tag{5}$$

We propose that the ECM emission excited by the energetic electron beam, trapped in the potential well of the SKAW, can be responsible for the weak SRBs, called SWR, and while the frequency drift of SWR is caused by the travel of the SKAW at the velocity $v_{sw} = \sqrt{(2 + n_m)/3n_m} v_A > v_A$. Specificly, a single small-scale weak SRB is attributed to a single SKAW.

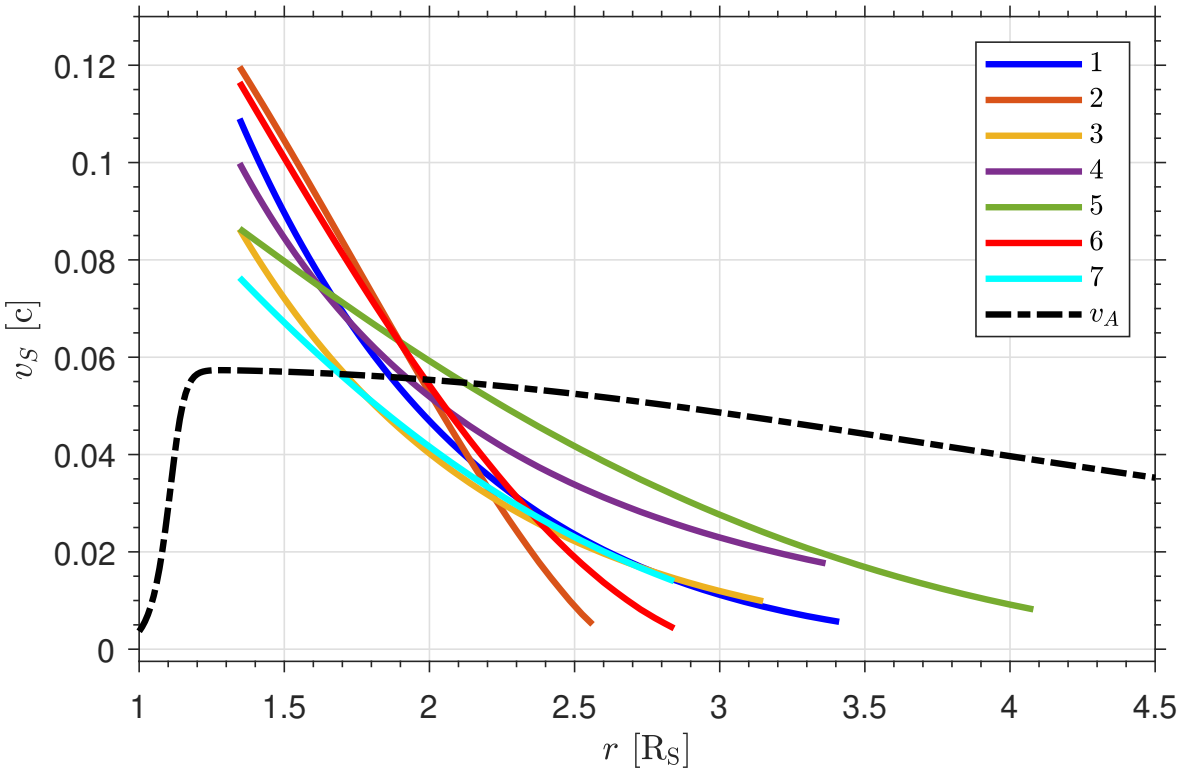

Figure 5. (color online) The radial distributions of the emitting source velocities for the typical events of weak SRBs v_S/c (solid lines) and the Alfvén velocity v_A/c (dashed line) along an open magnetic field region in the low-density magnetic channel, where all velocities have been normalized by the light speed c.

Combining the relative frequency-drifting rate D, presented in Figure 2(f), with the radial distribution of the electron cyclotron frequency f_{ce} (i.e., $D = (df_{ce}/dr)(v_S/f)$), Figure 5 shows the moving velocity of the emitting sources v_S/c versus the heliocentric distance (solid lines) for the several typical weak SRBs in Figure 2(b), where the local Alfvén velocity v_A/c is presented by the dashed line for the sake of comparison, with a typical value $v_A \sim 0.05c$ in the source region. The sources have initial velocities $v_S \sim 0.1c \sim 2v_A$ and then rapidly descend to $v_S < v_A$. Here, we point out that these weak SRBs were excited by the energetic electrons with velocity $v_b \sim 0.35c \sim 7v_A$ which are trapped in the potential well of SKAW with velocity $v_{sw} = v_S \sim 0.1c \sim 2v_A$ (for $n_m = 0.2$). From Figure 5 it can be found that the motion of these sources has a common evolutionary feature, that is, a rapid deceleration with the heliocentric distance from initial $v_S > v_A$ in the closer to the Sun to $v_S < v_A$ in further distances, implying that the emitting sources experience an evident and

lasting deceleration as their traveling outwards. This common feature can be reasonably explained by the evolving property of SKAWs due to the dissipation in low-β plasma (Wahlund et al. 1994; Voitenko & Goossens 2000; Wu et al. 2007).

In the initial stage of the SKAW formation, the energetic electrons with the characteristic oscillating velocity v_b, accelerated by the SKAW electric field, are trapped within the SKAW potential well and travel at the velocity v_{sw} together with the SKAW (Wu et al. 2007). It is these trapped energetic electrons that trigger SWR via the ECM mechanism, in which the transverse free energy required by exciting the ECM instability can be provided by the wave-particle scattering of AW turbulence. As propagating, the SKAW may loss energy due to various possible dissipations, such as the Coulomb collision or ion-acoustic turbulence (Wahlund et al. 1994; Voitenko & Goossens 2000; Wu et al. 2007). This leads to the deceleration of the SKAW, i.e., the emitting source, because the propagating velocity v_{sw} decreases as the dissipation of the SKAW. In the meantime, accompanying with the dissipation, the symmetry of the SKAW potential well is deformed and evolves into a shock-like structure, and in consequence the part energetic electrons may escape from the SKAW potential well, until the SKAW is exhausted when the inner density $n_m \to 1$ (Wahlund et al. 1994; Wu & Chao 2004). The energetic electrons escaping from the dissipated SKAW gradually merge into the local plasma environment with strong AW turbulence and the corresponding SWR has a wider spectral band and a slower drifting velocity, and ultimately travels together with the accelerated solar wind at a velocity much lower than the local Alfvén velocity as shown in Figure 5.

The dissipation time of SKAWs may be estimated approximately by the inverse of the damping rate $\gamma \sim 0.5\nu_e k_\perp^2 \lambda_e^2$ in the coronal plasma (Voitenko & Goossens 2000; Wu et al. 2007), where $\nu_e = 2.91 \times 10^{-6} n_e T_e^{-1.5} \ln\Lambda$ is the electron collision frequency and $\ln\Lambda$ is the Coulomb logarithm. Assuming the typical electron density $n_e \sim 10^5$ cm^{-3} and temperature $T_e \sim 150$ eV in the source region, one has $\ln\Lambda \sim 20$ and $\nu_e \sim 3.16 \times 10^{-3}$ Hz. In a low-β plasma of $v_A > v_{T_e}$, SKAWs have a characteristic width $\lambda_\perp \sim 2\pi\lambda_e$ (i.e., $k_\perp \lambda_e \sim 1$), where $\lambda_e \equiv c/\omega_{pe}$ is the electron inertial length (Chaston et al. 1999). In consequence, the damping rate is $\gamma \sim 1.58 \times 10^{-3}$ Hz, implying that the dissipation time of SKAWs typically is about ten minutes (i.e., $\tau \sim \gamma^{-1} \sim 600$ s). However, actual damping

rate in general can be higher than this collision damping, and hence the observed lifetime of SWR may be shorter than the estimation here. A single SKAW can contribute to a single burst and the energetic electrons trapped in the potential well of SKAW can gain energy by the acceleration of the SKAW electric field. The power of the SKAW may be estimated by the production of the Joule heating rate ($\mathbf{J}\cdot\mathbf{E}$) in the SKAW and the SKAW volume, that is, $Q_H \sim jE\lambda_\perp^2\lambda_\parallel \sim 2.9\times10^{11}$ W, where $j \sim en_{em}v_b$ and $E \sim E_m\sqrt{m_e/m_p}v_AB_0$ are the current density and the electric field in the SKAW. Here, the parallel scale of SKAW $\lambda_\parallel \sim 10^3\lambda_\perp$, the dimensionless parameters $n_m = 0.2$ (hence, $v_b \simeq 7.66v_A \sim 0.35c$) and $E_m = 3.5$ (Wu 2012; Wu & Chen 2020) have been assumed. The magnetic field $B_0 \simeq 1.12$ G is obtained from Eq. (3) for the normalized heliocentric distance $r = 2.5$ has been used. On the other hand, the rate of energy loss due to the radio emission may be estimated as $Q_R \sim P \triangle f R_{pb}^2/(Z_0L_{eff}^2\Gamma^2) \sim 1.4\times10^9$ W $\ll Q_H$ (i.e., $Q_R \sim 0.01\ Q_H$), where the effective antenna length $L_{eff} \sim 1$ m, capacitive gain factor $\Gamma = 0.32$, and impedance of free space $Z_0 = 377\ \Omega$ have been used (Pulupa et al. 2017; Jebaraj et al. 2023). Here, taking event 5 for example, we have adopted the averge power spectral density $P \sim 10^{-16}$ V^2/Hz, the frequency width $\triangle f \sim 10^6$ Hz, and the distance between PSP and emitting source $R_{pb} \sim 33.5\ R_S$. If we consider further the fact that the coherent radio radiation often is a strong anisotropic emission, the radiation will be only concentrated within a small flare angle which cross section is possible much smaller than R_{pb}^2. In consequence, Q_R will decrease further and become much smaller than Q_H. In fact, the energy loss via the radio radiation is only a very small part of the energy loss of the SKAW, and the major energy loss of the SKAW is due to the dissipation caused by the classical or abnormal collision.

4. SUMMARY AND DISCUSSION

In summary, we reported a kind of weak SRBs observed by PSP when crossing a low-density magnetic channel during its E02 phase. These weak SRBs have a weak intensity lower than 10^{-15} V^2/Hz, the relatively low starting frequency ($\sim$ 20 MHz) and a narrow frequency range from a few tens MHz to a few hundreds kHz, and an evolving and intermediate relative frequency-draft rate $D \equiv \mid (df/dt)/f \mid$ from $D > 0.01$/s to < 0.01/s. They can occur quite frequently (five bursts per hour) and the nature of their weak intensity indicates that they originate from small-scale emitting

sources. Based on the common empirical models for the solar coronal plasma, these small-scale emitting sources lied in the heliocentric distance between $\sim 1.1 - 6.1\ R_S$, a typical solar wind acceleration region. We proposed that SKAWs in kinetic scales, which are formed easily in the solar wind acceleration region with a low-β plasma environment, can be responsible for the small-scale emitting sources of these weak SRBs, called SWR (solitary wave radiation).

Although the radio radiation of SWR has insignificant impact on the space plasma environment, the kinetic-scale characteristic of their emitting sources has important implications on the dynamics of magnetic plasmas in the solar wind acceleration region. One of the unsolved problems in solar physics is the heating and acceleration mechanism of coronal plasmas into the solar wind in the extended corona from 1.1 to 10 R_S. The complexity of the extended coronal plasma both in the kinetics and dynamics is the result of the plasma density decreasing with the heliocentric distance as well as the complicated magnetic topology in coronal plasmas. The decrease of the density leads to the transition of the coronal plasma from a collisionally dominated plasma to nearly collisionless one. As a result, the kinetic wave-particle interaction process plays an important role in the heating and acceleration of the coronal plasmas. On the other hand, the fully ionized state of the hydrogen, the major solar atmospheric component, results in the impossibility to gain the physical information associated with the acceleration and heating processes via spectral line observations of the hydrogen, which is a main method of inferring the physical situation and processes in the potospere and chromosphere. Alternately, however, radio observations, especially the observations of radiation originating from small-scale emitting sources can provide us rich information of energetic electrons and their kinetic processes as well as of the ambient magnetic plasmas in the solar wind acceleration region.

The present research at PMO was supported by the Strategic Priority Research Program of the Chinese Academy of Sciences under grant No. XDB0560000, the National Natural Science Foundation of China (NSFC) under grant Nos. 42174195, 11873018 and 11790302, and supported by the Specialized Research Fund for State Key Laboratories. We acknowledge the NASA Parker Solar Probe Mission and the FIELDS team led by S. D. Bale and the SWEAP team led by J. C. Kasper for use of data; the International LOFAR Telescope team for usage of the data.

The FIELDS and SWEAP experiments on the Parker Solar Probe spacecraft were designed and developed under NASA contract NNN06AA01C. The data could be obtained on the website: https://spdf.gsfc.nasa.gov/pub/data/psp/. We thank the anonymous referee for the useful comments which led to an improved version of the manuscript.

REFERENCES

Bale, S. D., Goetz, K., Harvey, P. R., et al. 2016, SSRv, 204, 49

Bale, S. D., Badman, S. T., Bonnell, J. W., et al. 2019, Nature, 576, 237

Bryant, D. A. 1990, "Two theories of auroral electron acceleration" in Solar and Planetary Plasma Physics, Ed. In Buti (London: World Scientific), 58

Chaston, C. C., Carlson, C. W., Peria, W. J., Ergun, R. E., & McFadden, J. P. 1999, GRL, 26, 647

Chen, L., Wu, D. J., Zhao, G. Q., & Tang, J. F. 2017, JGR, 122, 35

Chen, L., Ma, B., Wu, D. J., et al. 2021, ApJL, 915, L22

Cranmer, S. R., & van Ballegooijen, A. A. 2005, ApJS, 156, 265

Cranmer, S. R., van Ballegooijen, A. A., & Edgar, R. J. 2007, ApJS, 171, 520

Esser, R., & Sasselov, D. 1999, ApJL, 521, L145

Esser, R., Fineschi, S., Dobrzycka, D., et al. 1999, ApJL, 510, L63

Fox, N. J., Velli, M. C., Bale, S. D., et al. 2016, SSRv, 204, 7

Goldreich, P., & Sridhar, S. 1995, ApJ, 438, 763

Halekas, J. S., Whittlesey, P., Larson, D. E., et al. 2020, ApJL, 246, 22

Harra, L., Brooks, D. H., Bale, S. D., et al. 2021, A&A, 650, A7

Hu, Y. Q., Esser, R., & Habbal, S. R. 1997, JGR, 102, 14661

Jebaraj, I. C., Krasnoselskikh, V., Pulupa, M., Magdalenic, J., & Bale, S. D. 2023, ApJL, 955, L20

Kasper, J. C., Abiad, R., Austin, G., et al. 2016, SSRv, 204, 131

Kasper, J. C., Klein, K. G., Lichko, E., et al. 2021, PRL, 127, 255101

Leblanc, Y., Dulk, G., & Bougeret, J. 1998, SoPh, 183, 165

Lin, R. P., Evans, L. G., & Fainberg, J. 1973, ApL, 14, 191

Louarn, P., Wahlund, J. E., Chust, T., et al. 1994, GRL, 21, 1847

Ma, B., Chen, L., Wu, D. J., & Bale, S. D. 2021, ApJL, 913, L1

Ma, B., Chen, L., Wu, D. J., Pulupa, M., & Bale, S. D. 2022, ApJL, 932, L26

Mariani, F., & Neubauer, F. M. 1990, in Physics of the Inner Heliosphere, ed. R. Schwenn & E. Marsch (New York: Springer), 183

McComas, D. J., Alexander, N., Angold, N., et al. 2016, SSRv, 204, 187

McComas, D. J., Christian, E. R., Cohen, C. M. S., et al. 2019, Natur, 576, 223

Melrose, D. B. 1980, SSRv, 26, 3

Morioka, A., Miyoshi, Y., Masuda, S., et al. 2007, ApJ, 657, 567

Morioka, A., Miyoshi, Y., Iwai, K., et al. 2015, ApJ, 808, 191

Mozer, F. S., Cattell, C. A., Hudson, M. K., et al. 1980, SSRv, 27, 155

Parker, E. N. 1958, ApJ, 128, 664

Pulupa, M., Bale, S. D., Bonnell, J. W., et al. 2017, JGR, 122, 2836

Pulupa, M., Bale, S. D., Badman, S. T., et al. 2020, ApJS, 246, 49

Reiner, M. J., & Kaiser, M. L. 1999, GRL, 26, 397

Stasiewicz, K., Bellan, P., Chaston, C., et al. 2000, SSRv, 92, 423

Tan, B. L., Chen, N., Yang, Y.-H., et al. 2019, ApJ, 885, 90

Teriaca, L., Poletto, G., Romoli, M., & Biesecker, D. 2003, ApJ, 588, 566

Tsurutani, B. T., Lakhina, G. S., Sen, A., Hellinger, P., et al. 2018, JGR, 123, 2458

Voitenko, Y., & Goossens, M. 2000, A&A, 357, 1073

Vourlidas, A., Howard, R. A., Plunkett, S. P., et al. 2016, SSRv, 204, 83

Wahlund, J.-E., Louarn, P., Chust, T., et al. 1994, GRL, 21, 1831

Wild, J. P., Roberts, J. A., & Murray, J. D. 1954, Nature, 173, 532

Wild, J. P. 1950, AJSR, A3, 541

Wu, D. J., & Chao, J. K. 2004, JGR, 109, A06211

Wu, D. J., & Chen, L. 2020, Kinetic Alfvén Waves in Laboratory, Space, and Astrophysical Plasmas, (Springer Press, Nanjing University Press)

Wu, D. J., & Fang, C. 2003, ApJ, 596, 656

Wu, D. J., & Yang, L. 2007, ApJ, 659, 1693

Wu, D. J., Wang, D. Y., & Fälthammar, C. G. 1995, PhPl, 2, 4476

Wu, D. J., Huang, J., Tang, J. F., & Yan, Y. H. 2007, ApJ, 665, L171

Wu, C. S., Wang, C. B., Wu, D. J., & Lee, K. H. 2012, PhPl, 19, 082902

Wu, D. J. 2012, Kinetic Alfvén Waves: Theory, Experiment, and Application (Beijing: Science Press)

Wu, D. J. 2014, PhPl, 21, 064506

Young, P. R., Klimchuk, J. A., & Mason, H. E. 1999, A&A, 350, 286

Zhao, G. Q., Feng, H. Q., & Wu, D. J. 2015, PhPl, 22, 102105